Food Hydrocolloids 79 (2018) 416–427

Contents lists available at ScienceDirect

Food Hydrocolloids

journal homepage: www.elsevier.com/locate/foodhyd

Microfibrillated cellulose addition improved the physicochemical and bioactive properties of biodegradable films based on soy protein and clove essential oil

Cristian Matías Ortiz [a], Pablo Rodrigo Salgado [a], Alain Dufresne [b], Adriana Noemí Mauri [a, *]

[a] Centro de Investigación y Desarrollo en Criotecnología de Alimentos (CIDCA), CONICET CCT La Plata y Facultad de Ciencias Exactas, Universidad Nacional de La Plata, 47 y 116 S/N°, B1900JJ La Plata, Argentina
[b] Université Grenoble Alpes, CNRS, LGP2, Grenoble INP, F-38000 Grenoble, France

ARTICLE INFO

Article history:
Available online 16 January 2018

Keywords:
Active nanocomposites films
Soybean protein
Microfibrillated cellulose
Clove essential oil
Antioxidant and antimicrobial properties

ABSTRACT

Active nanocomposite films based on soy protein isolates (SPI), microfibrillated cellulose (MFC) and clove essential oil (CEO) were developed, and the contribution of each component to the functionality of ensuing films was intended to elucidate. MFC with diameters of 50–60 nm, an average length of 485 ± 2 μm, a high aspect ratio of 8800 and 35.5% of cristalinity, was prepared from *Phormium tenax* fibers by mechanical treatment. Films were processed by casting from aqueous dispersions containing SPI, glycerol (as plasticizer), different MFC contents and the optional addition of CEO. All filmogenic dispersions exhibited a pseudoplastic flow behavior and formed homogeneous films. The addition of MFC reinforced the protein matrix, increasing the mechanical strength and Young's modulus of the films and improving their barrier properties to water vapor and oxygen. On the other hand, the addition of CEO caused some plastification effect of protein and nanocomposite matrix (mainly observed in the mechanical properties, solubility and water content) and a differential modification in the barrier properties, as the oxygen permeability increased and WVP decreased. Furthermore, it conferred important antioxidant properties and antimicrobial activity against bacteria related to foodborne diseases that increased with increasing MFC content in the formulation. Nanofibers seemed to favor the release of the active compounds of CEO probably due to the improved dispersion of CEO in nanocomposites through a higher amount of smaller droplets. These active nanocomposite films with antimicrobial and antioxidant properties are promising for the development of active food packaging.

1. Introduction

Nanocomposites may overcome the inherent shortcomings of biopolymer-based packaging materials. They show improved barrier and mechanical properties, as well as heat resistance compared to both their neat polymer matrix and conventional composites, even with the addition of a very low concentration of nanoreinforcement (<10%). Those based on nanoclays have been the most studied and gained the attention of the food industry to be used as packaging materials. However in the last decade numerous studies have also been devoted to the generation of nanoreinforcements derived from polysaccharides such as cellulose, starch and chitosan (Arora & Padua, 2010; Azeredo, 2009; Sorrentino, Gorrasi, & Vittoria, 2007).

Cellulose, a biodegradable, low cost and widely available material, can be used to prepare different types of nanoreinforcements. Microfibrillated cellulose (MFC) is used to designate long, flexible and entangled cellulose nanofibers (20–60 nm in diameter and several micrometers in length) with a high axial Young modulus (≈100 GPa) (Dufresne, 2012, p. 460). Unlike cellulose nanocrystals (CNC) obtained by acid hydrolysis, MFC has amorphous and crystalline domains (Lu, Wang, & Drzal, 2008). Its aspect ratio (L/d) is very high, which denotes a very low percolation threshold and an ability to form an advantageous rigid network (Lavoine, Desloges, Dufresne, & Bras, 2012). MFC can be produced by multi-pass high-pressure homogenization and direct mechanical fibrillation (Donsi, Wang, Li, & Huang, 2010; Henriksson,

* Corresponding author. Centro de Investigación y Desarrollo en Criotecnología de Alimentos (CIDCA), CONICET CCT La Plata y Facultad de Ciencias Exactas, Universidad Nacional de La Plata, 47 y 116 S/N°, B1900JJ La Plata, Argentina.
E-mail address: anmauri@quimica.unlp.edu.ar (A.N. Mauri).

https://doi.org/10.1016/j.foodhyd.2018.01.011
0268-005X/

Berglund, Isaksson, Lindström, & Nishino, 2008; Henriksson, Henriksson, Berglund, & Lindström, 2007; Li, Yue, & Liu, 2012; Wang et al., 2012).

MFC has been prepared from different sources, such as bleached paper pulp, Kraft paper pulp, eucalyptus wood pulp, wheat and rice straw, bagasse and cotton stalk fibers straw, palm rachis, carrots, among others (Adel et al., 2016; Guimarães et al., 2016; Hassan et al., 2015; Matsuda, Ueno, & Hirose, 2001; Wang et al., 2012; Zimmermann, Bordeanu, & Strub, 2010); and managed to improve the performance of numerous biopolymer films (Cheng, Wang, & Rials, 2009; Fujisawa, Saito, Kimura, Iwata, & Isogai, 2013; Li et al., 2014; Lu et al., 2008; Lönnberg, Larsson, Lindström, Hult, & Malmström, 2011; Qi, Yang, Jing, Fu, & Chiu, 2014; Siqueira, Bras, & Dufresne, 2010; Xu et al., 2013a,b; Yao et al., 2014), although no reports on their effects on soy protein films were found.

As far as we know, phormium (*Phormiun tenax*) fibers, employed mainly in the textile industry and largely cultivated in Argentina in the islands of the Delta formed by the Buenos Aires and Entre Ríos provinces, have not been used to prepare MFC, although they were used in composites (Newman, Clauss, Carpenter, & Thumm, 2007; Rosa, Santulli, & Sarasini, 2010), CNC preparation (Fortunati et al., 2013) and their respective nanocomposites (Fortunati et al., 2014).

Nanocomposites can be also used as carriers of active agents and controlled release systems in the field of active food packaging. The diffusion rate of active compounds through the material can be modified by differences in the polymer network crosslinking and the increased tortuosity of the road ahead, both caused by nanofiller's presence (Mascheroni, Chalier, Gontard, & Gastaldi, 2010). Although there are many works in which films based on biopolymers have been activated with different synthetic and natural active compounds from varied sources, there are not so many in which nanocomposite matrices based on proteins have been activated.

In previous works, nanocomposite films based on soy protein and montmorillonite nanoclay (MMT) were activated with important antioxidant and antimicrobial properties through the addition of clove essential oil (CEO, *Syzygium aromaticum* L.) to the formulation, that were used for the preservation of refrigerated bluefin tuna (*Thunnus thynnus*) fillets (Echeverría, López-Caballero, Gómez-Guillén, Mauri, & Montero, 2016; 2018). MMT appeared to facilitate the release of some active compounds, promoting the decrease of total volatile basic nitrogen (TVBN) index, the final count of microorganisms and lipid autoxidation of fish during chilled storage. It seemed that nanoclay's presence may favor the release of the active principles of clove oil by prolonging its antimicrobial and antioxidant activity over time.

The objectives of this work were to prepare biodegradable nanocomposites based on soybean proteins and phormium (*Phormium tenax*) MFC, activate them through CEO addition, and evaluate the role of each component in films' physicochemical and bioactive properties.

2. Materials and methods

2.1. Materials

A commercial soy protein isolate (SPI) SUPRO 500E, kindly supplied by DuPont N & H (Brazil), was used as biopolymer. The protein content of SPI, as measured by the Kjeldahl method, was 85 ± 2% (w/w on dry basis; N × 5.71). Phormium (*Phormium tenax*) fibers were purchased at Silkum (Argentina) and used as nanocellulose reinforcement source. Glycerol (Anedra, Argentina) was used as plasticizer in all the experiments. Clove (*Syzygium aromaticum* L.) essential oil (CEO Eladiet SA., Spain) was used to activate films. All the other reagents used in this study were of analytical grade.

2.2. Microfibrillated cellulose (MFC) preparation

Initially, *Phormium tenax* fibers were submitted to a washing pre-treatment to remove impurities and waxy substances covering the external surface of fiber cell walls. They were chopped to an approximate length of 5–10 mm and dispersed in 1 M NaOH (5% w/v) at 80 °C for 2 h using an overhead stirrer (OS20-Pro, DragonLab, China) at 500 rpm. The resulting suspension was filtered (270 mesh) and washed with cold water. This procedure was repeated twice. As lignin hinders fiber separation, partial delignification (bleaching) was performed in order to facilitate further cellulose nanofibers preparation. Pre-treated fibers were dispersed (5% w/v) in 3% v/v H_2O_2 at 80 °C at 500 rpm (OS20-Pro, DragonLab, China) for 30 min, then cooled in an ice bath, filtered (270 mesh) and washed with cold water. This procedure was also repeated twice. Bleached fibers were dried at 80 °C for 15 h in an oven with air flow circulation (Yamato, DKN600, USA).

Treated fibers were immersed in distilled water (1 wt % dry pulp) for 16 h and dispersed using a blender at 3125 rpm during 6 min. The resulting suspension was fibrillated using a high-shear ultrafine friction grinder Super Masscolloider (Masuko Sangyo Co, Japan). Size reduction of the cellulose fibers into nanoparticles was obtained after 50 passes between the rotating and the static stones at 1500 rpm. Solid content of the resulting MFC suspension was around 0.9% (w/w). MFC suspension was stored at 4 °C, after adding some drops of chloroform (10 drops/L) to avoid bacterial growth, until it was used.

2.3. Microfibrillated cellulose characterization

2.3.1. Morphology and diameter

The morphology of MFC samples was observed by Atomic Force Microscopy (AFM). A drop of diluted MFC aqueous suspension (0.01% wt) was dried on an optical glass substrate at room temperature and imaged in tapping mode with a Nanoscope IIIa microscope (Veeco Instruments Inc., China). MFC diameter was measured by Nanoscope software.

2.3.2. Length

It was automatically measured with a MorFi LB-01 fibre analyser (Techpap, France) by a computer analysis of images of the suspension flowing (fiber content of 0.300 g/L) through a flat cell observed by a digital CCD video-camera.

2.3.3. Crystallinity index (CI)

It was determined using an X-ray diffractometer X'Pert Pro (PANalytical, USA) with a monochromatic CuKα radiation source (λ = 0.1539 nm), 40 kV, 40 mA and sampling interval of 0.01. Scattered radiation was detected in the angular range 2θ = 5–60°. CI was calculated using Equation (1) (Segal, Creely, Martin, & Conrad, 1959):

$$CI = [(I_{002} - I_{am})/I_{002}] \times 100 \quad (1)$$

Where: I_{002} is the maximum intensity of the (002) lattice diffraction peak (around 2θ = 22°) and I_{am} is the intensity scattered by the amorphous part of the sample (around 2θ = 18°).

2.4. Film formation

Films were prepared by casting, after dispersing SPI (5% w/v), glycerol (25 g/100 g SPI) and different amounts of MFC (0, 4, 8, and

12 g/100 g SPI) in distilled water at room temperature (≅ 20 °C). Dispersions were stirred in a vertical stirrer with flat propellers (Dragon LAB OS20-PRO, China) at 150 rpm for 2.5 h at room temperature, and their pH was adjusted to 10.5 with 2 N NaOH. Finally CEO (50 g/100 g SPI) was added to some dispersions, according to Salgado, López-Caballero, Gómez-Guillén, Mauri, and Montero (2013) and Echeverría et al. (2016 and 2018). Aliquots (10 mL) of each filmogenic dispersion were poured on polystyrene Petri dishes (64 cm^2) and then dehydrated at 60 °C for 3 h in an oven with air flow circulation (Yamato, DKN600, USA). Protein and nanocomposite films with and without CEO were conditioned during 48 h at 20 °C and 58% relative humidity (RH) in desiccators with saturated solutions of NaBr before being peeled from the casting surface to be characterized.

2.5. Rheology of film-forming dispersions

Rotational analyses of film-forming dispersions were performed at 20 °C in a ReoStress 600 rheometer (Thermo Haake, Karlsruhe, Germany) with a 1 mm gap serrated plate–plate sensor (PP35 sensor). The shear rate (D) was increased from 0 to 500 s^{-1} in 2 min, it was maintained for 1 min and then decreased from 500 to 0 s^{-1} over a period of other 2 min. The apparent viscosity (η_{app}) was calculated in the ascending curves at 60 and 500 s^{-1}. The yield stress (τ_0), flow index (n) and consistency index (K) were determined after adjusting the empirical data according to the Herschel-Bulkley rheological model (Equation (2)):

$$\tau = \tau_0 + K\, D^n \quad (2)$$

Where: τ is the shear stress (Pa), τ_0 is the yield stress (Pa), K is the consistency index (Pa s^n), D is the shear rate (s^{-1}) and n is the flow index (dimensionless). Determinations were carried out in triplicate.

2.6. Films characterization

2.6.1. Thickness

Films thickness was measured with a digital coating thickness gauge (Check Line DCN-900, USA). Measurements for testing the mechanical and water-barrier properties were performed at ten different locations on the films. The average thickness was used to calculate these physical properties.

2.6.2. Color

Films color was determined using a Minolta Chroma meter (CR 300, Minolta Chroma Co., Osaka, Japan). A CIE Lab color scale was used to measure the degree of lightness (L), redness (+a) or greenness (-a), and yellowness (+b) or blueness (-b) of the films. The instrument was standardized using a set of three Minolta calibration plates. Films were measured on the surface of the white standard plate with color coordinates of $L_{standard} = 97.3$, $a_{standard} = 0.14$ and $b_{standard} = 1.71$. Total color difference (ΔE) was calculated from Equation (3):

$$\Delta E = [(L_{film} - L_{standard})^2 + (a_{film} - a_{standard})^2 + (b_{film} - b_{standard})^2]^{0.5} \quad (3)$$

Values were expressed as the means of nine measurements on different areas of each film.

2.6.3. Opacity

Each film specimen was cut into a rectangular piece (0.5 cm × 2 cm) and placed directly in a UV-vis spectrophotometer (Beckman DU650, Germany). Measurements were performed with air as the reference for transparency. A spectrum of each film was obtained in a UV–vis spectrophotometer (Beckman DU650, Germany). The area under the absorption curve from 400 to 800 nm was recorded and the opacity of the film (arbitrary units/mm) calculated by dividing the absorbance at 500 nm by the film's thickness (mm) (Condés, Añón, Mauri, & Dufresne, 2015). All determinations were performed in triplicate.

2.6.4. Moisture content (MC)

Small specimens of films (≈0.25 g) were collected after conditioning, cut, and weighed before and after drying in an oven at 105 °C until constant weight. Moisture content values were determined in triplicate as the difference between the two weights for each film and were expressed as a percent of the original weight (ASTM, 1994).

2.6.5. Water solubility (WS)

Film solubility was determined according to Gontard, Duchez, Cuq, and Guilbert (1994). Three film pieces (≈2 cm in diameter) were immersed in 50 mL distilled water and slowly stirred at room temperature (22–25 °C) for 24 h (Ferca, TT400 model, Argentina). After filtration of the samples (Whatman 1) the nonsolubilized material on the paper was dried in a forced-air oven (105 °C, 24 h) in order to determine the weight of the water-insoluble fraction as a percent of the total. WS was calculated and it was expressed in percentage. Measurements were done in triplicate.

2.6.6. Glass transition temperature

The glass-transition temperature (Tg) of the films was determined by differential scanning calorimetry, with a DSC TA2010 calorimeter Model Q100 V9.8 Build296 (TA Instrument, New Castle, DE, USA) equipped with a TA5000 temperature controller and a quench-cooling accessory. Temperature and heat-flow calibrations were carried out according to ASTM indications, with lauric acid, stearic acid, and indium as standards. Hermetically sealed aluminum pans containing 7–10 mg of films were prepared and scanned at 10 °C min^{-1} over the range −100 to 150 °C. The Tg was considered to be the inflexion point of the base line caused by the discontinuity of the specific heat of the sample (ASTM, 2004), and it was calculated by means of the Universal Analysis V4.2E software (TA Instruments, New Castle, DE, USA). All the assays were performed in at least duplicate.

2.6.7. Contact angle

Surface hydrophobicity was assessed by measuring the surface water contact angle at room temperature, using a goniometer (Ramé-Hart Model 250, Succasunna, USA). A 5 μl drop of demineralized water was placed on the surface of the film and the evolution of the droplet shape was recorded with a video camera. Image analyzer software (DROPimage Advanced v2.2) was used to measure the contact angle. The contact angles were measured on both sides of the drop and averaged. A minimum of ten measurements, taken at different positions on the film, were carried out.

2.6.8. Water vapor permeability (WVP)

WVP tests were conducted by the ASTM method E96-00 (ASTM E96-00, 1996) with certain modifications (Gennadios, McHugh, Weller, & Krochta, 1994). Each film sample was sealed over a circular opening of 0.00159 m^2 in a permeation cell that was subsequently stored at 20 °C in a desiccator. To maintain a 75% RH gradient across the film, anhydrous silica (0% RH_c) was placed inside the cell and a saturated NaCl solution (75% RH) in the desiccator. The RH therefore was always lower inside the cell than outside, and the water-vapor transport was accordingly determined from the weight gain of the permeation cell. When steady-

state conditions were reached (after about 1 h), eight weight measurements were made over a period of 7 h. Changes in the weight of the cell were recorded and plotted as a function of time. The slope of each line was calculated by linear regression (Origin Pro 8.5 software) and the water-vapor–transmission rate was calculated from the slope (g H_2O s^{-1}) divided by the cell area (m^2). WVP (g H_2O/Pa.s.m) was calculated as Equation (4):

$$WVP = [WVTR/(\mathbf{P_v^{H2O}}(RHd - RHc)\ A)]\ d \quad (4)$$

Where WVTR = the water-vapor–transmission rate, P_v^{H2O} = vapor pressure of water at saturation (1753.35 Pa) at the test temperature (20 °C), RH_d = RH in the desiccator, RH_c = RH in the permeation cell, A = permeation area, and d = film thickness (m). Each WVP value represents the mean value of at least three samples taken from different films.

2.6.9. Oxygen permeability (OP)

The oxygen transmission rate (OTR) was determined in an OX-TRAN 2/21 (Mocon, MN, USA) based on the ASTM D3985-02 method (ASTM, 2004). Test cell was composed of two chambers separated by the sample of 50 cm^2. On one side of the film 100% oxygen gas was flowing, and on the other side there was a flow of nitrogen gas (98% N_2 and 2% H_2). The RH of both gases was controlled at 65% by a humidifier. Measurements were made at 23 °C and atmospheric pressure (760 mm Hg). Oxygen permeability (OP) was calculated as Equation (5):

$$OP = (OTR/\Delta PO2)\ .\boldsymbol{d} \quad (5)$$

in which OTR is the oxygen transmission rate, ΔP_{O2} is the difference between oxygen partial pressure across the film and d is film's thickness.

Measurements were done in duplicate for film samples from each condition.

2.6.10. Mechanical properties

Film mechanical properties were determined by tensile tests according to the ASTM D882-02 method (ASTM, 2004) in a texture analyzer TA. XT2i (Stable Micro Systems, Surrey, England) equipped with a tension grip system A/TG, according to Salgado et al. (2011). Films were cut into strips (6 mm × 80 mm) that were mounted with two grips at opposite ends. Initial grip separation was 50 mm and the crosshead speed during the assay was 0.5 mm s^{-1}. The tensile strength and the elongation at break were determined directly from the stress-strain curves through the use of OriginPro 8 SR0 v8.0724 software (OriginLab Corporation, USA), and the Young's modulus was obtained from the slope of the initial linear portion of that curve. At least six measurements for each condition, using different films were performed.

2.6.11. Scanning electron microscopy (SEM)

Surface and cross-section area (cryofractured by immersion in liquid nitrogen) of films was observed by SEM. The pieces of films were mounted on aluminum stubs using a double-sided tape and were coated with a thin gold layer using a cool sputter system (SCD 005, Bal-Tec, Switzerland). SEM images were acquired with a scanning electron microscope (XL-20, Philips, Netherlands), using an acceleration voltage of 10 kV for all the samples. SEM image magnifications × 50 for film surface and × 300 for film cross-section are shown in this work.

2.6.12. Transmission electron microscopy (TEM)

Small pieces of film (0.5 mm^2) were fixed in 2.5% (v/v) glutaraldehyde in Sorenssen buffer (pH 7.2), washed in the same buffer three times for 30 min each, and then postfixed in 2% (w/v) OsO_4 for 1 h. The samples were next washed with distilled water three times for 30 min each, serially dehydrated in aqueous acetone (25%, 50%, 75%, and 100% [3 ×]), and finally embedded in Spurr Resin (1:2, 2:2, 2:1) and pure resin overnight. Polymerization was carried out at 70 °C overnight. The embedded samples were sectioned with an LKB ultramicrotome. The grids were stained with uranyl acetate (1 min) and lead-citrate (40 min) and observed with a JEOL 100CXII (Tokyo, Japan) transmission electron microscope at 80 kV.

2.6.13. Antioxidant properties

The supernatants obtained in WS test (Section 2.6.5) were used for testing the film's antioxidant capacity based on the $ABTS^{\bullet+}$ radical (2,2-azinobis-(3-ethylbenzothiazoline-6-sulfonic acid)) scavenging capacity (Salgado, Fernández, Drago, & Mauri, 2011).

The stock solution of $ABTS^{\bullet+}$ radical (7 mM of 2,2- azinobis-(-ethylbenzothiazoline-6-sulfonic acid) in 2.45 mM potassium persulfate) was kept in the dark at room temperature for 12–16 h. An aliquot of stock solution was diluted with buffer sodium phosphate 0.01 M at pH 7.4 to prepare the working solution of $ABTS^{\bullet+}$ radical with an absorbance of 0.70 ± 0.03 at 734 nm. (Beckman DU650, Alemania).

A 100 μl aliquot of the samples was mixed with 900 μl of ABTS reagent. The mixture was then left to stand at 30 °C for 6 min and absorbance values were read at 734 nm.

Results were expressed as mmol equivalent of gallic acid per gram of soluble film based on a standard curve relating the concentration of gallic acid (3,4,5-trihydroxybenzoic acid, Sigma-Aldrich, USA) to the degree of absorbance reduction caused by such acid. All determinations were performed in triplicate.

2.6.14. Antimicrobial activity

The antimicrobial activity of films was determined by the agar disk diffusion method against 4 microbial strains as described by Salgado et al., 2013. Briefly, edible films were cut into discs of 30 mm diameter and laid onto the surface of agar previously inoculated with 100 μL of each microorganism. The strains, selected by its importance in health or for being responsible for food spoilage, were obtained from the Centro de Investigación y Desarrollo en Criotecnología de Alimentos (CIDCA) collection, and included: *Bacillus cereus*, *Escherichia coli*, *Salmonella enteritidis* and *Staphylococcus aureus*. All the strains were grown in nutritious broth (Biokar Diagnostics, Francia). Organisms were incubated for 24 h at 37 °C. After incubation the inhibition (clear) area, considered as a measure of the antimicrobial activity, was determined with Adobe Acrobat® version 6 Professional software. Results were expressed as percentage of growth inhibition respecting to the total plate surface. Each determination was performed in triplicate.

2.7. Statistical analysis

Results are expressed as average ± standard deviation and were analyzed by analysis of variance (ANOVA). Averages were tested with the Tukey's honest significance test (HSD) for paired comparison, with a significance level $\alpha = 0.05$, using the SYSTAT v. 12 software (Systat Software, Inc., Chicago, USA).

3. Results and discussion

3.1. Phormium tenax microfibrillated cellulose

Fig. 1 shows the appearance of initial and pre-treated phormium fibers, the MFC suspension obtained at the end of the mechanical process, as well as the morphology of the resulting nanofibers analyzed by AFM. The raw phormium fibers, already cut (Fig. 1A)

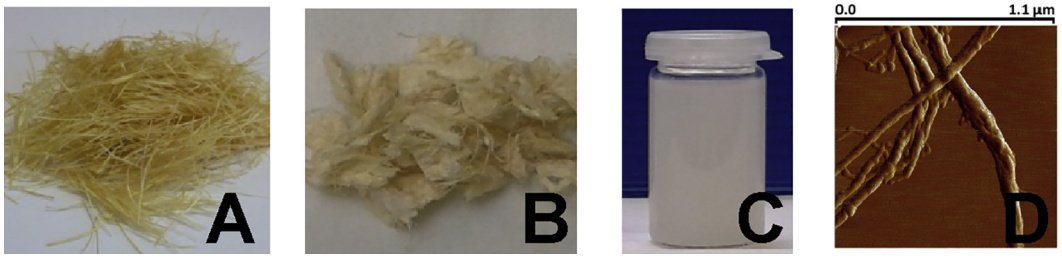

Fig. 1. Visual appearance of raw phormium fibers (*P. tenax*) (A), and after alkaline and bleaching treatments (B); of the MFC suspension (C) and atomic force microscopy (AFM) image of the resulting nanofibers (D).

showed a similar appearance to that published by other authors (Rosa et al., 2010) and some yellowish coloration, which was attenuated with the alkaline and bleaching pre-treatments used to remove part of hemicelluloses and lignin. These treated fibers also showed a stronger tendency to agglomerate (Fig. 1B).

The homogenization process to which the fibers were subjected led to an aqueous suspension with a weak gel appearance (Fig. 1C), that had a high stability since it did not flocculate or sediment for at least 2 years when stored at 4 °C. MFC observed by AFM (Fig. 1D) showed diameters around 50–60 nm, which allows to consider them as nanofibers. Their average length of 485 ± 2 μm (measured by light scattering) leads to an aspect ratio (L/d) of 8800, which constitutes one of the main structural differences with CNCs (Jonoobi et al., 2015) besides the crystallinity. Phormium MFC crystallinity index was of 35.5%, lower than the values reported for CNC (Flauzino Neto, Silvério, Dantas, & Pasquini, 2013; Lu & Hsieh, 2012; Xu et al., 2013b) and for MFC prepared from others resources, such as flax, rutabaga, and wood (59, 64 and 54%, respectively) (Bhatnagar & Sain, 2005; Lavoine et al., 2012).

3.2. Rheology of film forming dispersions

Table 1 summarizes the rheological characteristics for SPI film forming dispersions with different concentrations of MFC with and without clove essential oil (CEO). The experimental values for the shear stress as a function of strain rate gradient were satisfactorily adjusted to the Herschel-Bulkley model ($R > 0.99$). SPI dispersions showed a pseudoplastic flow behavior ($n < 1$) similar to that previously reported by other authors (Echeverría, Eisenberg, & Mauri, 2014). This rheological behavior was accentuated by the addition of increasing concentrations of MFC, as observed by the decline in the flow-behavior index (n) and the increase of the consistency index (K) and the apparent viscosity throughout the range of shear rates analyzed, but especially at lower shear rates. Apparent viscosity values at shear rates of 60 and 500 s^{-1} were compared in Table 1. The observed changes in the rheological behavior of the dispersions could be attributed to the increase in solid content in the formulation due to nanofiber addition, as well as to interactions between soybean proteins (SPI) and MFC, probably through hydrogen bonds (Siqueira et al., 2010), achieving a higher degree of packing (Lavoine et al., 2012). Although dispersions containing 12 g of MFC per 100 g of SPI exhibited high apparent viscosities (124.6 ± 2.5 mPa s at $D = 60\ s^{-1}$), their processing could be performed without inconvenience. Above this MFC concentration it was not possible to obtain homogeneous films since the high viscosities achieved complicated at once the admixture, the removal of bubbles, and the fluidity required for casting.

The incorporation of CEO into protein and nanocomposite formulations also increased the pseudoplastic flow behavior, except for films containing 4 g of MFC/100 g SPI whose sheer strength and apparent viscosity remained constant unexpectedly. But when increasing the MFC content, an important change in all parameters of filmogenic dispersions was observed (Table 1), probably due to the possible interactions among the different components SPI, MFC and CEO in the film forming dispersions (Burt, 2004; Echeverría, 2012, p. 275).

3.3. Soybean protein and MFC nanocomposite films added or not with CEO

3.3.1. Appearance

All the studied formulations allowed obtaining continuous, flexible and homogenous films, able to encapsulate CEO (50 g/100 g SPI) in the protein or nanocomposite networks, since no oily exudate neither oily appearance to touch was observed in the resulting materials.

Table 2 shows the values of thickness, opacity and color parameters for the studied films. The addition to protein formulations of increasing MFC contents and CEO led to a gradual increase in thickness and opacity. The large aspect ratio of MFC would contribute to increase the dispersion of light, increasing opacity (Yu et al., 2017). In contrast, Fortunati et al. (2014) reported that the

Table 1
Rheological characteristics for film forming dispersions from soy protein with increasing contents of MFC without or with CEO. Panel A: yield stress (τ_0), consistency index (K), and flow index (n) calculated using the Herschel-Bulkley model. Panel B: Apparent-viscosity values calculated at shear rates (D) of 60 and 500 s^{-1}.

Film	MFC (g/100 g SPI)	A. Parameters of Herschel-Bulkley model			B. Apparent viscosity (mPa s)	
		τ_0 (Pa)	K (Pa s^{-n})	n	$D = 60s^{-1}$	$D = 500s^{-1}$
SPI	0	0.09 ± 0.02^{e}	0.03 ± 0.01^{d}	0.87 ± 0.04^{a}	20.2 ± 1.2^{e}	15.3 ± 0.3^{g}
	4	1.23 ± 0.03^{c}	0.05 ± 0.01^{d}	0.80 ± 0.01^{bc}	46.9 ± 1.7^{d}	19.4 ± 0.4^{f}
	8	2.71 ± 0.04^{b}	0.08 ± 0.01^{d}	0.76 ± 0.01^{c}	80.8 ± 1.2^{c}	26.1 ± 0.3^{de}
	12	4.67 ± 0.17^{a}	0.18 ± 0.01^{c}	0.64 ± 0.01^{d}	124.6 ± 2.5^{b}	31.4 ± 0.6^{c}
SPI + CEO	0	0.54 ± 0.03^{d}	0.08 ± 0.01^{d}	0.81 ± 0.01^{bc}	49.1 ± 0.9^{d}	28.2 ± 0.3^{cd}
	4	1.20 ± 0.06^{c}	0.05 ± 0.01^{d}	0.83 ± 0.02^{ab}	47.6 ± 1.1^{d}	21.2 ± 1.1^{ef}
	8	3.20 ± 0.28^{b}	0.49 ± 0.07^{b}	0.54 ± 0.01^{e}	130.3 ± 1.5^{b}	36.7 ± 3.7^{b}
	12	4.17 ± 0.39^{a}	1.04 ± 0.06^{a}	0.44 ± 0.01^{f}	175.3 ± 1.1^{a}	44.5 ± 2.1^{a}

Values for each dispersion are average ± standard deviation. Values with different letters in a given column are significantly different ($p < .05$) according to the Tukey test.

Table 2
Thickness, color parameters (*L*, *a*, *b*, *ΔE*), and opacity for soy protein films with increasing contents of MFC without or with CEO.

Film	MFC (g/100 g SPI)	Thickness (μm)	Hunter-Lab color parameters				Opacity (UA/mm)
			L	*a*	*b*	*ΔE*	
SPI	0	64.8 ± 5.0^{e}	90.3 ± 0.8^{ab}	-2.5 ± 0.2^{c}	14.9 ± 1.4^{e}	15.7 ± 1.7^{d}	2.0 ± 0.1^{e}
	4	66.9 ± 5.2^{de}	90.6 ± 0.6^{a}	-2.9 ± 0.2^{cd}	15.7 ± 0.8^{e}	15.4 ± 1.0^{d}	2.4 ± 0.1^{d}
	8	69.1 ± 5.5^{cd}	89.3 ± 0.6^{bc}	-3.0 ± 0.1^{d}	17.7 ± 0.3^{d}	18.1 ± 0.5^{c}	3.6 ± 0.1^{c}
	12	71.9 ± 4.0^{bc}	88.6 ± 0.2^{c}	-3.1 ± 0.1^{d}	19.2 ± 0.1^{c}	19.8 ± 0.1^{c}	3.8 ± 0.1^{b}
SPI + CEO	0	67.6 ± 5.0^{de}	82.8 ± 1.4^{d}	1.9 ± 0.5^{b}	27.8 ± 1.3^{b}	30.1 ± 2.0^{b}	3.4 ± 0.2^{c}
	4	74.3 ± 5.7^{b}	81.4 ± 0.6^{e}	2.1 ± 0.1^{b}	28.1 ± 0.7^{b}	30.5 ± 1.4^{b}	3.9 ± 0.1^{b}
	8	81.9 ± 6.2^{a}	78.2 ± 0.9^{f}	3.5 ± 0.3^{a}	29.7 ± 0.3^{a}	34.1 ± 0.8^{a}	4.0 ± 0.1^{b}
	12	84.6 ± 7.2^{a}	77.8 ± 0.4^{f}	3.7 ± 0.1^{a}	29.8 ± 0.1^{a}	34.3 ± 0.3^{a}	4.4 ± 0.1^{a}

Values for each film are average ± standard deviation. Values with different letters in a given column are significantly different ($p < .05$) according to the Tukey test.

addition of CNC obtained from phormium fibers to poly (lactic acid) (PLA) films did not modify the transparency of the films, but these fibers were significantly smaller (L = 100–200 nm/d = 5–10 nm) and they were added up to only 3%. The presence of CEO in the protein matrix or nanocomposites would also generate a greater dispersion of light, increasing the film opacity (Prodpran, Benjakul, & Artharn, 2007) due to the difference in the refractive index of the phases and the particle size (Monedero, Fabra, Talens, & Chiralt, 2009; Pereda, Aranguren, & Marcovich, 2010; Pérez-Mateos, Montero, & Gómez-Guillén, 2009).

Soybean protein films showed their characteristic yellowish coloration (Echeverría et al., 2014) which was increased by the addition of MFC to the formulation (higher *b* and similar *a* and *L*). Moreover, CEO's presence led to a more orange coloration attributed to the joint increase in *a* and *b* parameters accompanied by a decrease of *L*. These changes in film color could be atributed to the own color of both components -MFC and CEO- and consequently provoked the increase in color variation (*ΔE*). Pereda et al. (2010) also observed an increase in the yellow coloration of casein films added with tung oil, which was attributed to the oil's own coloration.

3.3.2. Water susceptibility

The addition of MFC to the protein films did not affect the water content, the hydrophobicity (studied by the contact angle), or the glass transition temperature of the material, but caused a slight increase in water solubility for the samples with 8 and 12 g of MFC per 100 g of SPI (Table 3). It is clear that the presence of MFC does not change the hydrophilic nature of soy protein films, but they would be interfering with or modifying the cross-linking among polypeptide chains by the formation of new protein-fiber interactions, mainly by hydrogen bonds (Siró & Plackett, 2010), more susceptible to destabilization during the solubility test.

On the other hand, the addition of CEO increased both the water content and water solubility of the film without modifying its surface hydrophobicity. Oil should be well trapped in the protein and nanocomposite matrix, as mentioned above, since its hydrophobicity was not evidenced on films' surface. The well-known emulsifying properties of soybean proteins (Ventureira, 2010, p. 195) could explain these findings. During emulsification, proteins modify their conformation, exposing their hydrophobic groups around the oily drop, forming a film that stabilizes the emulsion, leaving the more hydrophilic centers for the formation of more soluble materials, with greater capacity to retain water and in some cases with lower contact angle against water. Different effects have been reported when adding essential oils to protein films. Thus, for example, Pereda et al. (2010) observed higher surface hydrophobicities by adding tung oil to casein protein films obtained by casting. Ahmad, Benjakul, Prodpran, and Agustini (2012) and Salgado et al. (2013) observed lower solubilities of gelatin and sunflower protein films added with bergamot and lemongrass or clove essential oils, respectively. In agreement with these results, Gómez-Estaca, López de Lacey, López-Caballero, Gómez-Guillén, and Montero (2010) and Pires et al. (2013) reported that the addition of citronella, thyme, coriander and clove essential oils to gelatin and gelatin-chitosan films increased their water solubility due to the formation of new interactions between proteins and essential oils, which weakened the protein network. Echeverría (2012, p. 275) also observed that adding clove essential oil to protein and nanocomposite films based on soy protein and MMT increased the water content of the films but did not modify their water solubility.

Nanofibers could also contribute to stabilize the emulsions keeping the oil dispersed in the nanocomposite matrix. The ability of nanoparticles such as MFC, CNC, or even starch nanocrystals to stabilize o/w emulsions by pickering has been reported (Capron & Cathala, 2013; Echeverría, 2012, p. 275; Kalashnikova, Bizot, Bertoncini, Cathala, & Capron, 2013; Kalashnikova, Bizot, Cathala, & Capron, 2011; Kargar, Fayazmanesh, Alavi, Spyropoulos, & Norton, 2012; Mikulcová, Bordes, & Kaspárková, 2016; Rayner et al., 2014; Tan et al., 2012; Tavernier, Wijaya, Van der Meeren, Dewettinck, & Patel, 2016; Winuprasith & Suphantharika, 2013).

No strong differences in the Tg of the films were observed with the addition of MFC or CEO (Table 3). It seems that changes in the

Table 3
Moisture content, solubility, water contact angle and glass transition temperature for soy protein films with increasing MFC contents with or without CEO.

Film	MFC (g/100 g SPI)	Moisture content (%)	Solubility (%)	Contact angle (°)	Tg (°C)
SPI	0	15.72 ± 0.30^{c}	32.12 ± 1.62^{f}	68.42 ± 0.91^{a}	-35.05 ± 4.60^{a}
	4	15.47 ± 0.15^{c}	33.17 ± 0.50^{ef}	63.35 ± 1.28^{c}	-34.14 ± 4.37^{a}
	8	15.40 ± 0.10^{c}	36.67 ± 1.79^{de}	67.60 ± 1.51^{ab}	-33.20 ± 3.54^{a}
	12	14.67 ± 0.13^{c}	37.46 ± 0.45^{cd}	63.20 ± 0.95^{c}	-31.96 ± 5.36^{a}
SPI + CEO	0	22.48 ± 0.60^{ab}	38.47 ± 0.63^{abc}	62.76 ± 1.38^{c}	-35.59 ± 0.19^{a}
	4	22.45 ± 0.43^{ab}	41.21 ± 0.28^{bcd}	63.07 ± 1.75^{c}	-31.62 ± 0.21^{a}
	8	21.86 ± 0.39^{b}	42.08 ± 2.15^{ab}	63.85 ± 1.94^{c}	-34.40 ± 0.02^{a}
	12	23.09 ± 0.59^{a}	43.46 ± 2.11^{a}	64.74 ± 0.49^{bc}	-31.07 ± 9.47^{a}

Values for each film are average ± standard deviation. Values with different letters in a given column are significantly different ($p < .05$) according to the Tukey test.

binding pattern caused by the presence of both components (oil and nanofibers) did not modify the mobility of the polypeptide chains. In contrast, other authors observed an increase in the Tg value for MFC nanocomposites, which was attributed to a homogeneous dispersion of the nanofibers in the polymer matrix that could restrict the mobility of polymer chains (Mukherjee et al., 2014).

3.3.3. Barrier properties

The water vapor and oxygen permeabilities (WVP and OP, respectively), and the oxygen transmission rate (OTR) of the studied films are shown in Table 4. Protein films (without MFC and CEO) showed a WVP value characteristic of hydrophilic materials ($13.90 \pm 0.32 \times 10^{-11}$ g H_2O m^{-1} Pa^{-1} s^{-1}), in the same range of values published elsewhere (Gennadios, 2002). The addition of MFC to the protein formulation decreased the WVP value for films containing 8 and 12 g of MFC per 100 g of SPI. This effect could be associated with a successful dispersion of the nanofibers within the protein matrix that produced a more tortuous path for the passage of water molecules through the film (Tunc et al., 2007).

The addition of CEO to the formulation also provoked a decrease in WVP of protein and nanocomposites films, achieving lower WVP values by increasing the nanofiber content in the formulation. This effect would be related to the oily nature of CEO and to the good dispersion of the oil in the protein or nanocomposite matrix that could increase the tortuosity of the way to go through the film of water molecules. It would also overcome the opposite effect produced by the higher water content in films containing CEO, which would favor the passage of water molecules through the material increasing WVP.

It should also be noted that when lipids are dispersed in a polymer matrix their effect on WVP depends on a number of factors, such as lipid type and concentration, hydrophobicity, particle size and emulsion stability (Debeaufort & Voilley, 1995; Pérez-Gago & Krochta, 2001). Thus, there are examples in which the addition of essential oil did not modify the WVP value for protein films, or even increase it slightly (Ahmad et al., 2012; Giménez, Gómez-Guillén, López-Caballero, Gómez-Estaca, & Montero, 2012; Salgado et al., 2013) and others in which it is reduced (Pelissari, Grossmann, Yamashita, & Pineda, 2009; Pereda et al., 2010) as in this work. For activated nanocomposite matrices, Echeverría et al. (2016) did not observe any modification in the WVP value when adding clove essential oil to SPI-MMT films.

SPI control films (without MFC and CEO) showed a low OP (48.97 ± 1.92 mL O_2 μm m^{-2} day^{-1} kPa^{-1}), similar to other protein films (Ramos et al., 2013; Weizman, Dotan, Nir, & Ophir, 2017). The oxygen transmission rate (OTR) through the film decreased progressively when increasing the MFC content in the formulation (Table 4), but this effect was not appreciated in the OP of the film (Table 4), probably due to the effect of thickness in this measurement, since it increased as the MFC content increased. The decrease in OTR could also be attributed to the more tortuous path for the passage of oxygen molecules due to the presence of the nanofibers and to their crystalline nature. Plackett et al. (2010), observed a decrease in OP by adding MFC to amylopectin films, while Syverud and Stenius (2009) and Dufresne (2012, p. 460) reported that the high crystallinity of cellulose contributes to good barrier properties because the crystalline region would be practically impermeable to oxygen molecules.

Despite numerous attempts, it was not possible to measure the OP value for pure SPI films and those containing 4 g MFC per 100 g SPI added with CEO, because they were broken during the conduct of the test. However, adding CEO results in a significant increase in the OP value for films containing 8 and 12 g of MFC per 100 g of SPI. The OTR for these films also increased by 100 and 183%, respectively. This effect could be attributed to the hydrophobic nature of O_2 and consequently to its greater affinity with the essential oil and to a certain plasticizing effect that both the essential oil and the higher water content (Table 3) could cause, favoring the gas diffusion processes through the film (Dufresne, 2012, p. 460; Plackett et al., 2010).

3.3.4. Mechanical properties

Fig. 2 shows the mechanical properties for soybean protein films with increasing MFC contents with and without CEO, obtained from tensile tests. The addition of MFC improved the tensile strength and Young's modulus of protein films, to the detriment of their elongation. These properties changed significantly by 755, 1443 and 12%, respectively, when adding 8 g MFC/100 g SPI to protein film, but no significant differences were observed with those containing 12 g of MFC/100 g of SPI. This important reinforcing effect observed for films containing above 8 g of MFC per 100 g of SPI suggests that a percolation phenomenon of nanofibers in the protein matrix could occur, leading to the formation of a continuous cellulose nanoparticle network linked through hydrogen bonds immersed in the protein film, responsible for increasing the mechanical resistance of the nanocomposites (Samir, Alloin, & Dufresne, 2005; Dufresne, 2008a,b). Lu and Drzal (2010) reported a similar behavior working when investigating MFC-polyvinyl alcohol (PVA) nanocomposites and mentioned the existence of a limit load quantity, above which the fibers would begin to aggregate, leading to a reduction in the tensile strength and elastic modulus of the material.

The presence of CEO caused the opposite effect, i.e. a decrease in the tensile strength and Young's modulus without modifying the elongation at break. These results would confirm the plasticizing effect of the essential oil in the protein and nanocomposite films, as suggested before when analyzing their oxygen permeability that could be attributed at least partially, to the higher water content of these films. Several authors have reported the plasticizing effect of

Table 4
Permeability to water vapor (WVP), oxygen transmission rate (OTR) and permeability to oxygen (OP) for soy protein films with increasing MFC contents without or with CEO (n/d = no data).

Film	MFC (g/100 g SPI)	WVP × 10^{-11} (g H_2O/m Pa s)	OP (mL O_2 μm/m^2 day kPa)	OTR (mLO_2/m^2 day)
SPI	0	13.90 ± 0.32^{a}	48.97 ± 1.92^{b}	88.88 ± 3.42^{c}
	4	14.60 ± 0.41^{a}	52.32 ± 0.61^{b}	79.00 ± 0.74^{d}
	8	08.90 ± 0.65^{b}	47.07 ± 2.13^{b}	68.26 ± 2.51^{e}
	12	09.77 ± 0.36^{b}	47.88 ± 1.54^{b}	62.81 ± 1.85^{e}
SPI + CEO	0	09.66 ± 0.56^{b}	n/d	n/d
	4	09.24 ± 0.11^{b}	n/d	n/d
	8	06.89 ± 0.24^{c}	113.30 ± 3.20^{a}	136.93 ± 0.10^{a}
	12	07.12 ± 0.56^{c}	106.62 ± 3.25^{a}	115.00 ± 2.63^{b}

Values for each film are average ± standard deviation. Values with different letters in a given column are significantly different ($p < .05$) according to the Tukey test.

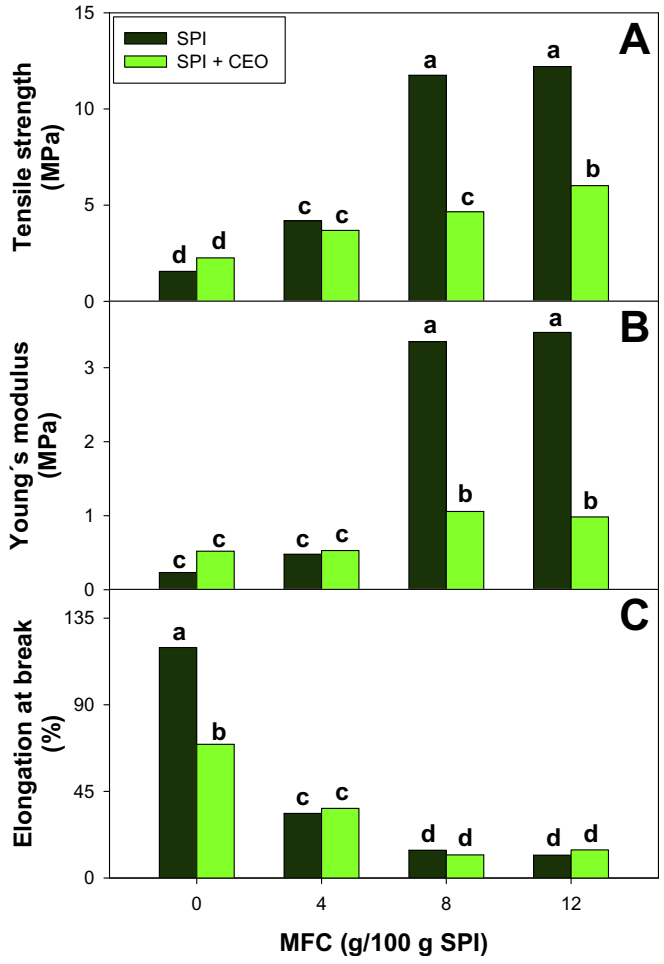

Fig. 2. Tensile strength (A), Young's modulus (B) and elongation at break (C) for soy protein films with increasing MFC content without or with CEO. Different letters indicate significant differences ($p < .05$) according to the Tukey test.

some essential oils on protein films (Andreuccetti, Carvalho, & Grosso, 2009; Bertan, Tanada-Palmu, Siani, & Grosso, 2005; Monedero, Fabra, Talens, & Chiralt, 2009; 2010; Pelissari et al., 2009), while others observed other behaviors (Fabra, Talens, & Chiralt, 2008; Pereda et al., 2010). Echeverría (2012, p. 275) also observed the plasticizing effect of clove essential oil in nanocomposite films prepared from SPI and MMT, and that the clay was able to improve the mechanical properties of the materials added with CEO, as in this work. But neither the reinforcement effect performed by the MFC, nor the plasticizer one caused by CEO, were noted when analyzing the Tg of the materials (Table 3).

3.3.5. Morphology

The morphology of the films was analyzed by SEM and TEM observations. Fig. 3 shows the surface and cross-sectional area of films with different MFC contents added or not with CEO. All films had a compact and dense microstructure which would imply a good affinity of all the components present in the formulation. Since it is not possible to visualize the MFC by SEM because of its low resolution, images would give at least an idea about the presence of aggregates of these nanofibers (Krishnamachari, Hashaikeh, & Tiner, 2011). For both the surface and cross-sectional area it is observed that MFC aggregates -marked with black arrows- and traces of CEO drops -marked with white arrows-are well dispersed and adhered to the protein matrix. Anywise, these micrographs would explain the reinforcing and plasticizing effects of MFC and CEO, respectively, mentioned above.

The presence of CEO seems to soften the nanocomposite surface, hides the presence of the nanofibers in those areas, whereas the oil droplets appeared to be smaller and therefore better dispersed in the protein matrix with 8 and 12 g of MFC/100 g SPI. Taking into account that the nanofibers could act as emulsifiers (Kalashnikova et al., 2011; 2013), probably MFC could contribute to a better dispersion of CEO in the protein matrix (Capron & Cathala, 2013; Kargar et al., 2012; Mikulcová et al., 2016; Rayner et al., 2014; Tan et al., 2012; Tavernier et al., 2016; Winuprasith & Suphantharika, 2013).

Fig. 4 shows the micrographs obtained by TEM nanocomposite films containing 12 g of MFC/100 g of SPI added or not with CEO. In the absence of CEO, MFC seems to be dispersed in the protein matrix but with some degree of aggregation possibly due to a concentration effect. However, when adding CEO, this aggregation was not clearly observed and the traces of CEO's drops interacting with the protein matrix and/or MFC nanofibers could interfere.

3.3.6. Antioxidant properties

Antioxidant properties of soybean protein films and their MFC nanocomposites, added or not with CEO, were evaluated in vitro by the $ABTS^{+}$ assay, and results are shown in Fig. 5. Protein and nanocomposite films, regardless of their MFC content, showed a very low antioxidant activity. The addition of CEO to the formulation significantly increased the antioxidant capacity of the films, which should be atributed to the oil's own phenolic compounds, mainly eugenol, gallic acid and caffeic acid (Dudonné, Vitrac, Coutiére, Woillez, & Mérillon, 2009). However, nanocomposite films with MFC contents from 8 g MFC/100 g SPI showed a significantly higher antioxidant activity. These results evidenced that in these materials the release of active compounds would be favor. This effect could be attributed to a better dispersion of CEO in nanocomposite films, to the macro structure of the fibers in these films and to the different bond pattern in these systems.

The facts that the presence of nanofibers led to a higher amount of smaller droplets of CEO (as was observed by SEM), and/or the increased in the viscosity of film forming dispersions with CEO addition (observed by rheology studies), led to suppose a emulsifying stabilizing effect caused by the fibers. In addition, some recently published studies have probed the ability of some nanoparticles, including cellulose nanofibers, to stabilize emulsions by pickering (Zhai, Lin, Liu & Yang, 2018; Chen, Zheng, Xu, Yin, Liu & Tang, 2018; Zhang, Y., Chen, Z., Bian, W., Feng, L., Wu, Z., Wang, P., Zeng & Wu, 2015). This effects contributes to a better dispersion of CEO in the nanocomposite film which could be consider as a higher effective concentration although all the studied films were prepared adding the same concentration of CEO.

3.3.7. Antimicrobial properties

Soybean protein films with different MFC contents and without CEO did not show antimicrobial activity. However, the addition of CEO to protein and nanocomposite films yields them an important antimicrobial activity against *Bacillus cereus*, *Escherichia coli*, *Salmonella enteritidis* and *Staphylococcus aureus* (Fig. 6), microorganisms that cause foodborne diseases and selected for possible application of these materials for food packaging. The antimicrobial activity was also progressively increased by increasing the MFC content, also suggesting that nanofibers would facilitate the release of CEO's active compounds, possibly due to a better dispersion of the oil in the nanocomposite matrix, causing a greater availability (Winuprasith & Suphantharika, 2013; 2015). A comparative study between the antimicrobial capacity of emulsions stabilized by CNCs and MFCs was done by Mikulcová et al. (2016), who compared

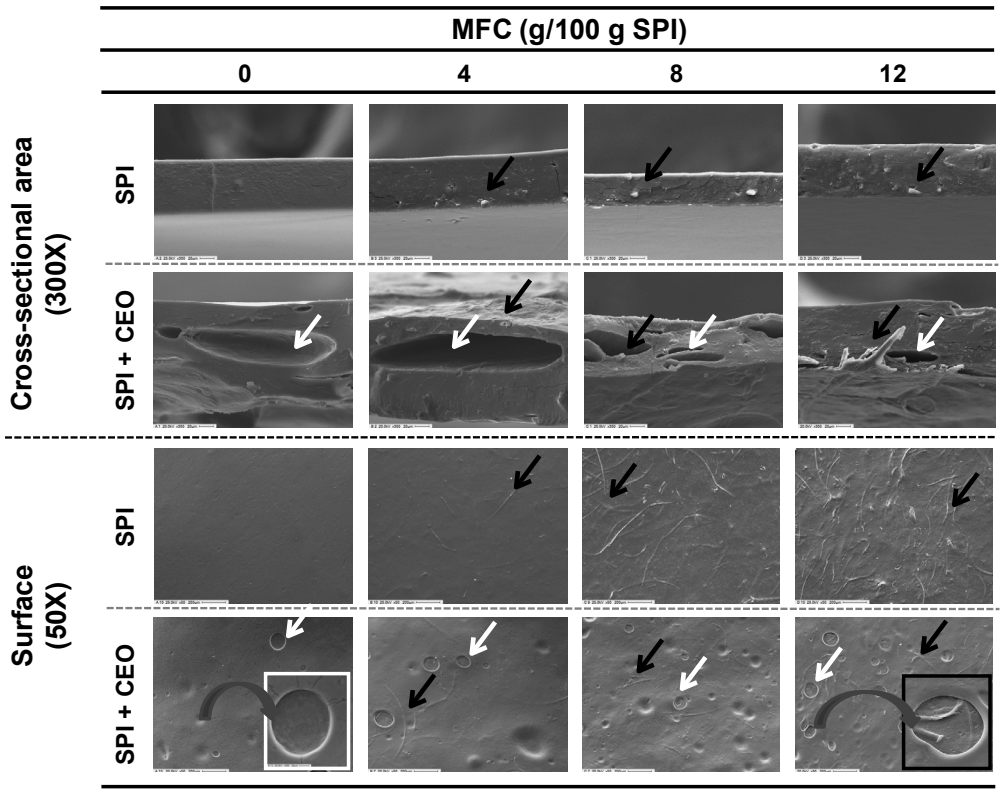

Fig. 3. Scanning electron microscopy (SEM) images of protein films with increasing MFC content without or with CEO. The presence of MFC aggregates (black arrow), together with the sites occupied by CEO (white arrow) is indicated.

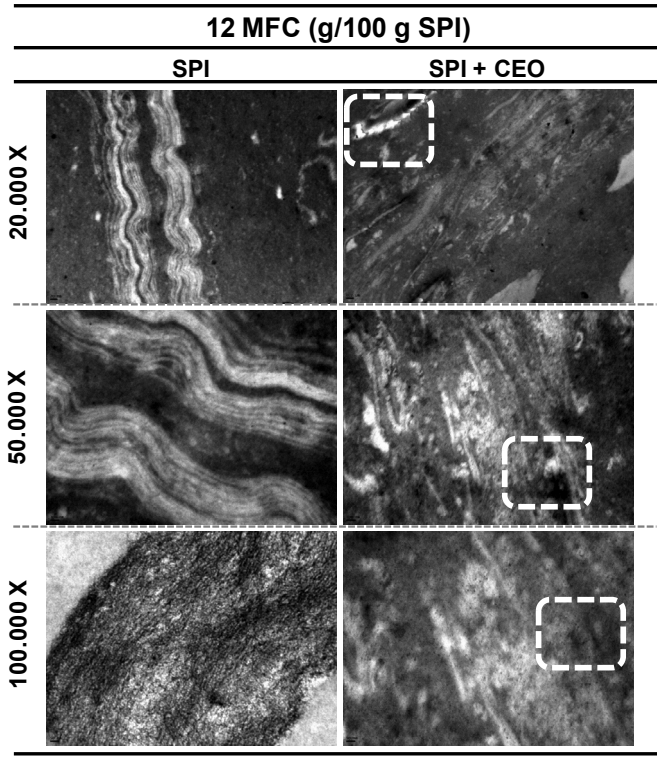

Fig. 4. Transmission electron microscopy (TEM) images of soy protein films reinforced with 12.0 g MFC/100 g SPI without and with addition of CEO. The presence of traces of the CEO drops (white dotted box) is indicated.

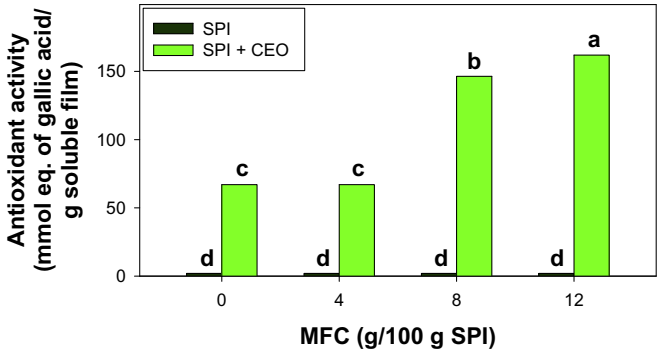

Fig. 5. Antioxidant activity of soy protein films with increasing MFC content without or with CEO. Different letters indicate significant differences ($p < .05$) according to the Tukey test.

pickering emulsions with three different antimicrobial oils (cinnamaldehyde, eugenol and limonene), and they showed that systems stabilized by MFC presented greater antimicrobial activities.

B. cereus was the most vulnerable strain against CEO's antimicrobial activity, followed by *S. aureus* and *E. coli.* A higher effectiveness of essential oils against *Gram*-positive bacteria such as *B. cereus* and *S. aureus* has been reported (Burt, 2004; Zivanovic, Chi, & Draughom, 2005). Zivanovic et al. (2005) proposed that the phenolic compounds present in essential oils could interact with the phospholipids membrane, increasing its permeability, allowing the leakage of cellular components of the cytoplasm, or interacting with enzymes located in the cell wall so affecting the correct metabolism of the microorganism. *Gram*-negative bacterias, such as *E. coli* and *Salmonella*, have an additional lipopolysaccharide

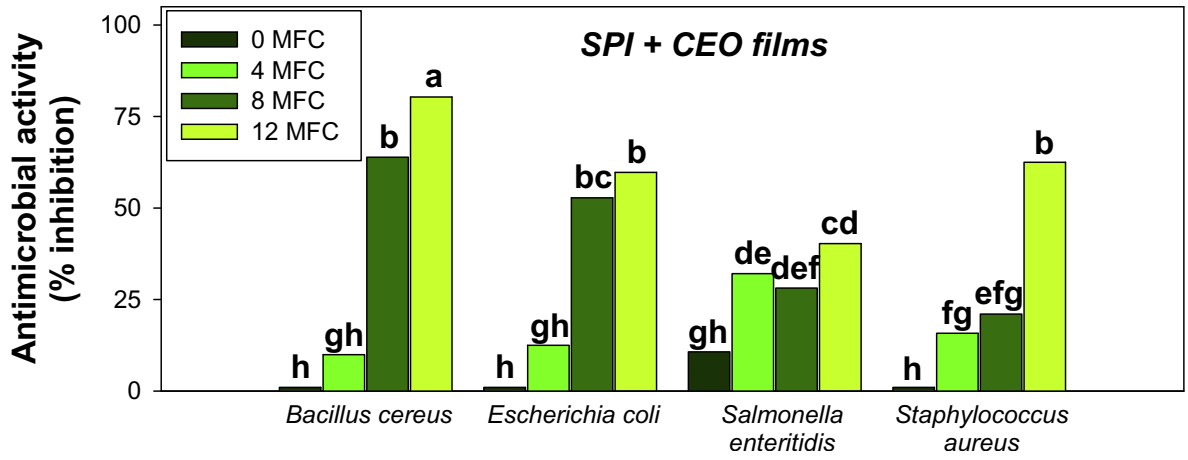

Fig. 6. Antimicrobial activity evaluated in *B. cereus*, *E. coli*, *S. enteritidis* and *S. aureus* represented as % inhibition of soy protein films with increasing MFC content without or with CEO. Different letters indicate significant differences ($p < .05$) according to the Tukey test.

outer membrane surrounding the cell wall, which would restrict the diffusion of hydrophobic compounds from the oil (Burt, 2004).

4. Conclusions

It was possible to obtain MFC from phormium fibers by a mechanical treatment. These nanofibers incorporated in soybean protein films achieved a strong reinforcing effect which was visualized through improvement in the mechanical and barrier properties without greatly modifying the appearance and Tg of the materials. These improvements could be attributed to the good compatibility between MFC and soybean proteins and to the possible formation of a nanofiber network embedded in the protein matrix, which could already be formed for formulations containing up to 8% MFC.

The addition of CEO to protein and MFC-nanocomposite films activated them with important antioxidant and antimicrobial properties and caused some plastification effect of the matrix (mainly observed in the mechanical properties, solubility and water content) and a differential modification in the barrier properties, as the oxygen permeability increased and WVP decreased.

MFC's presence seemed to favor the release of the active compounds of CEO. Increasing the concentration of MFC in films showed an increase in the antioxidant properties as well as the antimicrobial activity of the films against different bacteria of importance in foodborne diseases. These higher activities could be correlated with a better distribution of the CEO in the presence of MFC, through a higher amount of smaller droplets, that could probably be related to the own emulsifying effect of nanofibres, recently reported. These results excite about the use of these active nanocomposite materials in food preservation, which will be evaluated in future studies.

Acknowledgments

The authors would like to thank the National Agency of Scientific and Technological Support of Argentina (ANPCyT, PICT-2010-1837, PICT-2013-2124), La Plata National University (UNLP, Project 11/X618 and 11/X750) and to the CNRS (France) - CONICET (Argentina) Cooperation Project (2012) for their financial support.

References

Adel, A. M., El-Gendya, A. A., Diaba, M. A., Abou-Zeida, R. E., El-Zawawya, W. K., & Dufresne, A. (2016). Microfibrillated cellulose from agricultural residues. Part I: Papermaking application. *Industrial Crops and Products, 93*, 161–174.

Ahmad, M., Benjakul, S., Prodpran, T., & Agustini, T. W. (2012). Physico-mechanical and antimicrobial properties of gelatin film from the skin of unicorn leatherjacket incorporated with essential oils. *Food Hydrocolloids, 28*, 189–199.

Andreuccetti, C., Carvalho, R. A., & Grosso, C. R. F. (2009). Effect of hydrophobic plasticizers on functional properties of gelatin-based films. *Food Research International, 42*, 1113–1121.

Arora, A., & Padua, G. W. (2010). Nanocomposites in food packaging. *Journal of Food Science, 75*, R43–R49.

ASTM. (1994). *Annual book of ASTM standards*. Philadelphia, PA, USA: ASTM International.

ASTM. (2004). *Annual book of ASTM standards*. Philadelphia, PA, USA: ASTM International.

ASTM E96-00. (1996). Standard test methods for water vapor transmission of materials. In *Annual book of ASTM*. Philadelphia, PA: USA.

Azeredo, H. M. C. (2009). Nanocomposites for food packaging applications. *Food Research International, 42*, 1240–1253.

Bertan, L. C., Tanada-Palmu, P. S., Siani, A. C., & Grosso, C. R. F. (2005). Effect of fatty acids and 'Brazilian elemi' on composite films based on gelatin. *Food Hydrocolloids, 19*, 73–82.

Bhatnagar, A., & Sain, M. (2005). Processing of cellulose nanofiber reinforced composites. *Journal of Reinforced Plastics and Composites, 24*, 1259–1268.

Burt, S. (2004). Essential oils: Their antibacterial properties and potential applications in foods e a review. *International Journal of Food Microbiology, 94*, 223–253.

Capron, I., & Cathala, B. (2013). Surfactant free high internal phase emulsion stabilized by cellulose nanocrystals. *Biomacromolecules, 14*, 291–296.

Cheng, Q., Wang, S., & Rials, T. G. (2009). Poly(vinyl alcohol) nanocomposites reinforced with cellulose fibrils isolated by high intensity ultrasonication. *Composites Part A: Applied Science and Manufacturing, 40*, 218–224.

Chen, Q. H., Zheng, J., Xu, Y. T., Yin, S. W., Liu, F., & Tang, C. H. (2018). Surface modification improves fabrication of pickering high internal phase emulsions stabilized by cellulose nanocrystals. *Food Hydrocolloids, 75*, 125–130.

Condés, M. C., Añón, M. C., Mauri, A. N., & Dufresne, A. (2015). Amaranth protein films reinforced with maize starch nanocrystals. *Food Hydrocolloids, 47*, 146–157.

Debeaufort, F., & Voilley, A. Z. (1995). Effect of surfactants and drying rate on barrier properties of emulsified films. *International Journal of Food Science and Technology, 30*, 183–190.

Donsi, F., Wang, Y., Li, J., & Huang, Q. (2010). Preparation of curcumin submicrometer dispersions by high-pressure homogenization. *Journal of Agricultural and Food Chemistry, 58*, 2848–2853.

Dudonné, S., Vitrac, X., Coutiére, P., Woillez, M., & Mérillon, J. M. (2009). Comparative study of antioxidant properties and total phenolic content of 30 plant extracts of industrial interest using dpph, abts, frap, sod, and orac assays. *Journal of Agricultural and Food Chemistry, 57*, 1768–1774.

Dufresne, A. (2008). Cellulose-based composites and nanocomposites. In A. Gandini, & M. N. Belgacem (Eds.), *Monomers, polymers and composites from renewable resources* (pp. 401–418). Great Britain.

Dufresne, A. (2008). Polysaccharide nanocrystals reinforced nanocomposites. *Canadian Journal of Chemistry, 86*, 484–494.

Dufresne, A. (2012). *Nanocellulose: From nature to high performance tailored materials*. Berlin/Boston: Walter de Gruyter GmbH.

Echeverría, I. (2012). *Materiales biodegradables en base a proteínas de soja y montmorillonitas*. Doctoral Thesis. National University of La Plata.

Echeverría, I., Eisenberg, P., & Mauri, A. N. (2014). Nanocomposites films based on soy proteins and montmorillonite processed by casting. *Journal of Membrane Science, 449*, 15–26.

Echeverría, I., López-Caballero, M. E., Gómez-Guillén, M. C., Mauri, A. N., & Montero, M. P. (2016). Structure, functionality, and active release of nanoclay–soy protein films affected by clove essential oil. *Food and Bioprocess Technology, 9*, 1937–1950.

Echeverría, I., López-Caballero, M. E., Gómez-Guillén, M. C., Mauri, A. N., & Montero, M. P. (2018). Active nanocomposite films based on soy proteins-montmorillonite- clove essential oil for the preservation of refrigerated bluefin tuna (*Thunnus thynnus*) fillets. *International Journal of Food Microbiology, 266*, 142–149.

Fabra, M. J., Talens, P., & Chiralt, A. (2008). Tensile properties and water vapor permeability of sodium caseinate films containing oleic acidbeeswax mixtures. *Journal of Food Engineering, 85*, 393–400.

Flauzino Neto, W. P., Silvério, H. A., Dantas, N. O., & Pasquini, D. (2013). Extraction and characterization of cellulose nanocrystals from agro-industrial residue - soy hulls. *Industrial Crops and Products, 42*, 480–488.

Fortunati, E., Luzi, F., Puglia, D., Dominici, F., Santulli, C., Kenny, J. M., et al. (2014). Investigation of thermo-mechanical, chemical and degradative properties of PLA-limonene films reinforced with cellulose nanocrystals extracted from Phormium tenax leaves. *European Polymer Journal, 56*, 77–91.

Fortunati, E., Puglia, D., Monti, M., Peponi, L., Santulli, C., & Kenny, J. M. (2013). Extraction of cellulose nanocrystals from *Phormium tenax* fibres. *Journal of Polymers and the Environment, 21*, 319–328.

Fujisawa, S., Saito, T., Kimura, S., Iwata, T., & Isogai, A. (2013). Surface engineering of ultrafine cellulose nanofibrils toward polymer nanocomposite materials. *Biomacromolecules, 14*, 1541–1546.

Gennadios, A. (2002). *Protein-based films and coatings*. Boca Raton, FL: CRC Press LLC. USA.

Gennadios, A., McHugh, T. H., Weller, C. L., & Krochta, J. M. (1994). Edible coating and films based on protein. In *Edible coatings and films to improve food quality* (pp. 201–277). Lancaster, Pennsylvania: Technomic Publishing.

Giménez, B., Gómez-Guillén, C., López-Caballero, M. E., Gómez-Estaca, J., & Montero, P. (2012). Role of sepiolite in the release of active compounds from gelatin-egg white films. *Food Hydrocolloids, 27*, 475–486.

Gómez-Estaca, J., López de Lacey, A., López-Caballero, M. E., Gómez-Guillén, M. C., & Montero, P. (2010). Biodegradable gelatin-chitosan films incorporated with essential oils as antimicrobial agents for fish preservation. *Food Microbiology, 27*, 889–896.

Gontard, N., Duchez, C., Cuq, J. L., & Guilbert, S. (1994). Edible composite films of wheat gluten and lipids: Water vapour permeability and other physical properties. *International Journal of Food Science and Technology, 29*, 39–50.

Guimarães, I. C., dos Reis, K. C., Menezes, E. G. T., Rodrigues, A. C., da Silva, T. F., de Oliveira, I. R. N., et al. (2016). Cellulose microfibrillated suspension of carrots obtained by mechanical defibrillation and their application in edible starch films. *Industrial Crops and Products, 89*, 285–294.

Hassan, M. L., Bras, J., Mauret, E., Fadel, S. M., Hassan, E. A., & El-Wakil, N. A. (2015). Palm rachis microfibrillated cellulose and oxidized-microfibrillated cellulose for improving paper sheets properties of unbeaten softwood and bagasse pulps. *Industrial Crops and Products, 64*, 9–15.

Henriksson, M., Berglund, L. A., Isaksson, P., Lindström, T., & Nishino, T. (2008). Cellulose nanopaper structures of high toughness. *Biomacromolecules, 9*, 1579–1585.

Henriksson, M., Henriksson, G., Berglund, L. A., & Lindström, T. (2007). An environmentally friendly method for enzyme-assisted preparation of microfibrillated cellulose (MFC) nanofibers. *European Polymer Journal, 43*, 3434–3441.

Jonoobi, M., Oladi, R., Davoudpour, Y., Oskman, K., Dufresne, A., Hamzeh, Y., et al. (2015). Different preparation methods and properties of nanostructured cellulose from various natural resources and residues: A review. *Cellulose, 22*, 935–969.

Kalashnikova, I., Bizot, H., Bertoncini, P., Cathala, B., & Capron, I. (2013). Cellulosic nanorods of various aspect ratios for oil in water Pickering emulsions. *Soft Matter, 9*, 952–959.

Kalashnikova, I., Bizot, H., Cathala, B., & Capron, I. (2011). New Pickering emulsions stabilized by bacterial cellulose nanocrystals. *Langmuir: The ACS Journal of Surfaces and Colloids, 27*, 7471–7479.

Kargar, M., Fayazmanesh, K., Alavi, M., Spyropoulos, F., & Norton, I. T. (2012). Investigation into the potential ability of Pickering emulsions (food-grade particles) to enhance the oxidative stability of oil-in-water emulsions. *Journal of Colloid and Interface Science, 366*, 209–215.

Krishnamachari, P., Hashaikeh, R., & Tiner, M. (2011). Modified cellulose morphologies and its composites; SEM and TEM analysis. *Micron, 42*, 751–761.

Lavoine, N., Desloges, I., Dufresne, A., & Bras, J. (2012). Microfibrillated cellulose - its barrier properties and applications in cellulosic materials: A review. *Carbohydrate Polymers, 90*, 735–764.

Li, W., Wu, Q., Zhao, X., Huang, Z., Cao, J., Li, J., et al. (2014). Enhanced thermal and mechanical properties of PVA composites formed with filamentous nanocellulose fibrils. *Carbohydrate Polymers, 113*, 403–410.

Li, W., Yue, J., & Liu, S. (2012). Preparation of nanocrystalline cellulose via ultrasound and its reinforcement capability for poly(vinyl alcohol) composites. *Ultrasonics Sonochemistry, 19*, 479–485.

Lönnberg, H., Larsson, K., Lindström, T., Hult, A., & Malmström, E. (2011). Synthesis of polycaprolactone-grafted microfibrillated cellulose for use in novel bionanocomposites-influence of the graft length on the mechanical properties. *ACS Applied Materials and Interfaces, 3*, 1426–1433.

Lu, J., & Drzal, L. T. (2010). Microfibrillated cellulose/cellulose acetate composites: Effect of surface treatment. *Journal of Polymer Science Part B: Polymer Physics, 48*, 153–161.

Lu, P., & Hsieh, Y.-L. (2012). Preparation and characterization of cellulose nanocrystals from rice straw. *Carbohydrate Polymers, 87*, 564–573.

Lu, J., Wang, T., & Drzal, L. T. (2008). Preparation and properties of microfibrillated cellulose polyvinyl alcohol composite materials. *Composites: Part A, 39*, 738–746.

Mascheroni, E., Chalier, P., Gontard, N., & Gastaldi, E. (2010). Designing of a wheat gluten/montmorillonite based system as carvacrol carrier: Rheological and structural properties. *Food Hydrocolloids, 24*, 406–413.

Matsuda, Y., Hirose, M., & Ueno, K. (2001). *Super microfibrillated cellulose, process for producing the same and coated paper and tinted paper using the same*. US Patent. US: Tokushu Paper Mfg. Co., Ltd..

Mikulcová, V., Bordes, R., & Kaspárková, V. (2016). On the preparation and antibacterial activity of emulsions stabilized with nanocellulose particles. *Food Hydrocolloids, 61*, 780–792.

Monedero, F. M., Fabra, M. J., Talens, P., & Chiralt, A. (2009). Effect of oleic acid–beeswax mixtures on mechanical, optical and water barrier properties of soy protein isolate based films. *Journal of Food Engineering, 91*, 509–515.

Monedero, F. M., Fabra, M. J., Talens, P., & Chiralt, A. (2010). Effect of calcium and sodium caseinates on physical characteristics of soy protein isolate-lipid films. *Journal of Food Engineering, 97*, 228–234.

Mukherjee, T., Czaka, M., Kao, N., Gupta, R. K., Choi, H. J., & Bhattacharya, S. (2014). Dispersion study of nanofibrillated cellulose based poly(butyleneadipate-co-terephthalate) composites. *Carbohydrate Polymers, 102*, 537–542.

Newman, R. G., Clauss, E. C., Carpenter, J. E. P., & Thumm, A. (2007). Epoxy composites reinforced with deacetylated *Phormium tenax* leaf fibres. *Composites: Part A, 38*, 2164–2170.

Pelissari, F. M., Grossmann, M. V. E., Yamashita, F., & Pineda, E. A. G. (2009). Antimicrobial, mechanical, and barrier properties of cassava starch-chitosan films incorporated with oregano essential oil. *Journal of Agricultural and Food Chemistry, 57*, 7499–7504.

Pereda, M., Aranguren, M. I., & Marcovich, N. E. (2010). Caseinate films modified with tung oil. *Food Hydrocolloids, 24*, 800–808.

Pérez-Gago, M. B., & Krochta, J. M. (2001). Lipid particle size effect on water vapor permeability and mechanical properties of whey protein/beeswax emulsion films. *Journal of Agricultural and Food Chemistry, 49*, 996–1002.

Pérez-Mateos, M., Montero, P., & Gómez-Guillén, M. C. (2009). Formulation and stability of biodegradable films made from cod gelatin and sunflower oil blends. *Food Hydrocolloids, 23*, 53–61.

Pires, C., Ramos, C., Teixeira, B., Batista, I., Nunes, M. L., & Marques, A. (2013). Hake proteins edible films incorporated with essential oils: Physical, mechanical, antioxidant and antibacterial properties. *Food Hydrocolloids, 30*, 224–231.

Plackett, D., Anturi, H., Hedenqvist, M., Ankerfors, M., Gällstedt, M., Lindström, T., et al. (2010). Physical properties and morphology of films prepared from microfibrillated cellulose and microfibrillated cellulose in combination with amylopectin. *Journal of Applied Polymer Science, 117*, 3601–3609.

Prodpran, T., Benjakul, S., & Artharn, A. (2007). Properties and microstructure of protein-based film from round scad (*Decapterus maruadsi*) muscle as affected by palm oil and chitosan incorporation. *International Journal of Biological Macromolecules, 41*, 605–614.

Qi, X., Yang, G., Jing, M., Fu, Q., & Chiu, F.-C. (2014). Microfibrillated cellulose-reinforced bio-based poly(propylene carbonate) with dual shape memory and self-healing properties. *Journal of Materials Chemistry A, 2*, 20393–20401.

Ramos, Ó. L., Reinas, I., Silva, S. I., Fernandes, J. C., Cerqueira, M. A., Pereira, R. N., et al. (2013). Effect of whey protein purity and glycerol content upon physical properties of edible films manufactured therefrom. *Food Hydrocolloids, 30*, 110–122.

Rayner, M., Marku, D., Eriksson, M., Sjöö, M., Dejmek, P., & Wahlgren, M. (2014). Biomass-based particles for the formulation of Pickering type emulsions in food and topical applications. *Colloids and Surfaces A, 458*, 48–62.

Rosa, I. M. D., Santulli, C., & Sarasini, F. (2010). Mechanical and thermal characterization of epoxy composites reinforced with random and quasi-unidirectional untreated *Phormium tenax* leaf fibers. *Materials and Design, 31*, 2397–2405.

Salgado, P. R., Fernández, G. B., Drago, S. R., & Mauri, A. N. (2011). Addition of bovine plasma hydrolysates improves the antioxidant properties of soybean and sunflower protein-based films. *Food Hydrocolloids, 25*, 1433–1440.

Salgado, P. R., López-Caballero, M. E., Gómez-Guillén, M. C., Mauri, A. N., & Montero, M. P. (2013). Sunflower protein films incorporated with clove essential oil have potential application for the preservation of fish patties. *Food Hydrocolloids, 33*, 74–84.

Samir, A. M. A., Alloin, F., & Dufresne, A. (2005). Review of recent research into cellulosic whiskers, their properties and their application in nanocomposite field. *Biomacromolecules, 6*, 612–626.

Segal, L., Creely, J. J., Martin, A. E., & Conrad, C. M. (1959). An empirical method for estimating the degree of crystallinity of native cellulose using the X-ray diffractometer. *Textile Research Journal, 29*, 786–794.

Siqueira, G., Bras, J., & Dufresne, A. (2010). Cellulosic bionanocomposites: A review of preparation, properties and applications. *Polymers, 2*, 728–765.

Siró, I., & Plackett, D. (2010). Microfibrillated cellulose and new nanocomposite materials: A review. *Cellulose, 17*, 459–494.

Sorrentino, A., Gorrasi, G., & Vittoria, V. (2007). Potential perspectives of bionanocomposites for food packaging applications. *Trends in Food Science & Technology, 18*, 84–95.

Syverud, K., & Stenius, P. (2009). Strength and barrier of MFC films. *Cellulose, 16*, 75–85.

Tan, Y., Xu, K., Liu, C., Li, Y., Lu, C., & Wang, P. (2012). Fabrication of starch-based nanospheres to stabilize Pickering emulsion. *Carbohydrate Polymers, 88*, 1358–1363.

Tavernier, I., Wijaya, W., Van der Meeren, P., Dewettinck, K., & Patel, A. R. (2016). Food-grade particles for emulsion stabilization. *Trends in Food Science & Technology, 50*, 159–174.

Tunc, S., Angellier, H., Cahyana, Y., Chalier, P., Gontard, N., & Gastaldi, E. (2007). Functional properties of wheat gluten/montmorillonite nanocomposite films processed by casting. *Journal of Membrane Science, 289*, 159–168.

Ventureira, J. L. (2010). *Propiedades estructurales y funcionales de preparados proteicos de amaranto modificados y soja-amaranto*. Doctoral Thesis. National University of La Plata.

Wang, Q. Q., Zhu, J. Y., Gleisner, R., Kuster, T. A., Baxa, U., & McNeil, S. E. (2012). Morphological development of cellulose fibrils of a bleached eucalyptus pulp by mechanical fibrillation. *Cellulose, 19*, 1631–1643.

Weizman, O., Dotan, A., Nir, Y., & Ophir, A. (2017). Modified whey protein coatings for improved gas barrier properties of biodegradable films. *Polymers for Advanced Technologies, 28*, 261–270.

Winuprasith, T., & Suphantharika, M. (2013). Microfibrillated cellulose from mangosteen (*Garcinia mangostana* L.) rind: Preparation, characterization, and evaluation as an emulsion stabilizer. *Food Hydrocolloids, 32*, 383–394.

Winuprasith, T., & Suphantharika, M. (2015). Properties and stability of oil-in-water emulsions stabilized by microfibrillated cellulose from mangosteen rind. *Food Hydrocolloids, 43*, 690–699.

Xu, X., Liu, F., Jiang, L., Zhu, J. Y., Haagenson, D., & Wiesenborn, D. P. (2013). Cellulose nanocrystals vs. cellulose nanofibrils: A comparative study on their microstructures and effects as polymer reinforcing agents. *ACS Applied Materials & Interfaces, 5*, 2999–3009.

Xu, H., Xie, L., Chen, Y.-H., Huang, H.-D., Xu, J.-Z., Zhong, G.-J., et al. (2013). Strong shear flow-driven simultaneous formation of classic shish-kebab, hybrid shish-kebab, and transcrystallinity in poly(lactic acid)/natural fiber biocomposites. *ACS Sustainable Chemistry & Engineering, 1*, 1619–1629.

Yao, X., Qi, X., He, Y., Tan, D., Chen, F., & Fu, Q. (2014). Simultaneous reinforcing and toughening of polyurethane via grafting on the surface of microfibrillated cellulose. *ACS Applied Materials and Interfaces, 6*, 2497–2507.

Yu, Z., Alsammarraie, F. K., Nayigiziki, F. X., Wang, W., Vardhanabhuti, B., Mustapha, A., et al. (2017). Effect and mechanism of cellulose nanofibrils on the active functions of biopolymer-based nanocomposite films. *Food Research International, 99*, 166–172.

Zhai, D., Lin, D., Liu, D., & Yang, X. (2018). Emulsions stabilized by nanofibers from bacterial cellulose: New potential food-grade Pickering emulsions. *Food Research International, 103*, 12–20.

Zhang, Y., Chen, Z., Bian, W., Feng, L., Wu, Z., Wang, P., et al. (2015). Stabilizing oil-in-water emulsions with regenerated chitin nanofibers. *Food Chemistry, 183*(15), 115–121.

Zimmermann, T., Bordeanu, N., & Strub, E. (2010). Properties of nanofibrillated cellulose from different raw materials and its reinforcement potential. *Carbohydrate Polymers, 79*, 1086–1093.

Zivanovic, S., Chi, S., & Draughom, A. F. (2005). Antimicrobial activity of chitosan films enriched with essential oils. *Journal of Food Science, 70*, 45–51.